An Investigation of Ductility Dip Cracking in Nickel-Based Weld Metals — Part II

Fracture behavior and fracture surface morphology are related to microstructure, composition, and temperature

BY M. G. COLLINS, A. J. RAMIREZ, AND J. C. LIPPOLD

ABSTRACT. In Part I of this investigation of ductility dip cracking (DDC) in nickel-based filler materials (Ref. 1), the strain-to-fracture (STF) test was used to quantify the DDC susceptibility of two Ni-based filler metals, Filler Metal 52 and Filler Metal 82. Ductility dip cracking susceptibility was related to the nature of the migrated grain boundaries in these weld metal deposits and the influence of grain boundary composition and "tortuosity" on resistance to DDC. In Part II of this investigation, the fracture behavior and fracture surface morphology associated with DDC are related to composition, microstructure, and the temperature at which cracking occurs. This work is based on the evaluation of the fracture paths and surfaces in STF samples tested over the full DDC temperature range.

Fracture morphology was a strong function of temperature within the ductility dip temperature range (DTR) of 650–1200°C (1200–2190°F). At low and high temperatures within this range, fracture occurred by a ductile intergranular mode with clear evidence of ductile dimple rupture with sharp features at the grain faces. In the intermediate temperature range (850–1050°C), the fracture morphology is described as ductile intergranular with rounded features. In this range, the rounded ductile intergranular features were usually accompanied by slip intersections on the fracture surface that are manifested as serrated, terrace-like steps.

The nature of the carbides along the weld metal migrated grain boundaries had a strong influence on fracture behavior. In Filler Metal 82, the presence of numerous MC-type carbides (carbides of Nb, Ta, Ti, or V) resulted in more tortuous grain boundaries and higher resistance to cracking. The addition of hydrogen to the weld metal through the shielding gas had a profound negative effect on resistance to cracking. Cracking was widespread at grain boundary triple junctions under relatively low applied strains (less than 2%), exhibiting a macroscopically intergranular flat fracture surface. When these samples were tested at intermediate temperatures within the DDC range, they presented some unique regions with evidence of ductile fracture with relatively deep voids and porelike features.

This paper provides an overview of DDC fracture behavior in Ni-based filler metals and is a prelude to Part III of this investigation, which discusses the mechanism of DDC.

M. G. COLLINS, A. J. RAMIREZ, and J. C. LIPPOLD are with The Ohio State University, Columbus, Ohio.

KEY WORDS

Ductility Dip Cracking
Nickel-Based Filler Metals
Stain-to-Fracture Test
Grain Boundary Characteristics
Fracture Morphology

Introduction

Ductility dip cracking occurs below the effective solidus temperature, and separation of grain boundaries has been reported to be characteristic of materials susceptible to DDC (Refs. 2, 3). Part I of this investigation (Ref. 1) quantified DDC susceptibility in Filler Metal 52 and Filler Metal 82. Additionally, hydrogen and sulfur additions to the weld metal were evaluated with the STF test and were found to increase weld metal DDC susceptibility. Strain-to-fracture behavior was characterized by strain vs. temperature plots that showed the minimum strain required to initiate DDC in the weld metal microstructure. As part of the overall investigation, considerable characterization of microstructure and fracture morphology was conducted using the scanning electron microscope (SEM). Part II of this investigation focuses on the fracture characteristics of STF samples of both Filler Metals 52 and 82 over the entire DTR.

Experimental Procedures

Advanced characterization was conducted on STF samples of both Filler Metals 52 and 82. The compositions of these filler metals are provided in Table 1. The STF tests were performed in a Gleeble™ thermal-mechanical simulator according to the techniques reported in Part I. The STF test determined the cracking susceptibility of the alloys for specific strains and temperatures, which allowed development of DDC susceptibility curves for Filler Metals 52 and 82, also presented in Part I. In this investigation, SEM was used to characterize the fracture behavior of STF samples by examining DDC fracture surfaces both in the as-tested condition and after cleaning to remove surface oxidation.

Fracture surface analysis was conducted using both the Philips™ XL-30-FEG and Philips ultrahigh resolution Sirion-FEG SEMs. Saw cuts were made from all sides, using a water-cooled abrasive saw and a jeweler's saw, to isolate the cracks in the STF samples. The remaining ligament was then broken, and the fractured sample was ultrasonically cleaned in ethyl alcohol and dried in an oven at 60°C prior to insertion into the SEM. Samples were evaluated in both the as-tested condition and following ultrasonic cleaning for 30 min in an inhibited acid solution consisting of 3 mL of HCl, 4 mL of 2-butyne-1, 4-diol (35% aqueous solution), and 50 mL of deionized water. This technique proved very effective in removing the surface oxide without damaging the underlying fracture surface. Additionally, select samples were ultrasonically cleaned using the same acid solution for longer periods (up to 2 h), resulting in a minor etching effect and exposure of small precipitates upon the surface.

Metallographic samples for optical microscopy were prepared using standard pol-

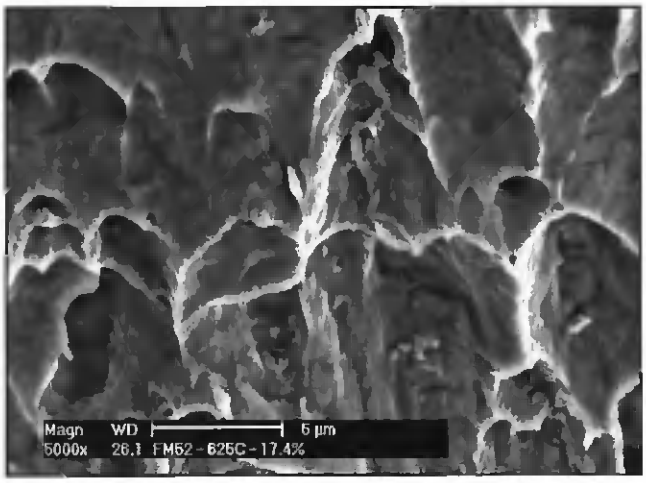

Fig. 1 — Filler Metal 52 fractograph at 625°C and 17% strain (5000×).

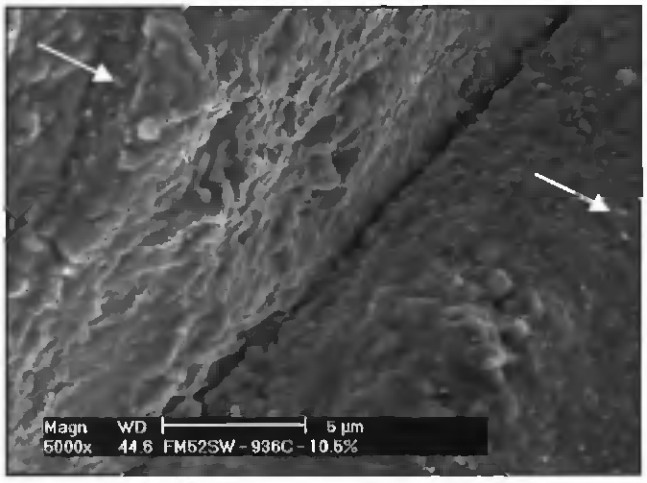

Fig. 2 — Filler Metal 52 fractograph at 936°C and 10.5% strain (5000×; arrows indicate small particles on the fracture surface).

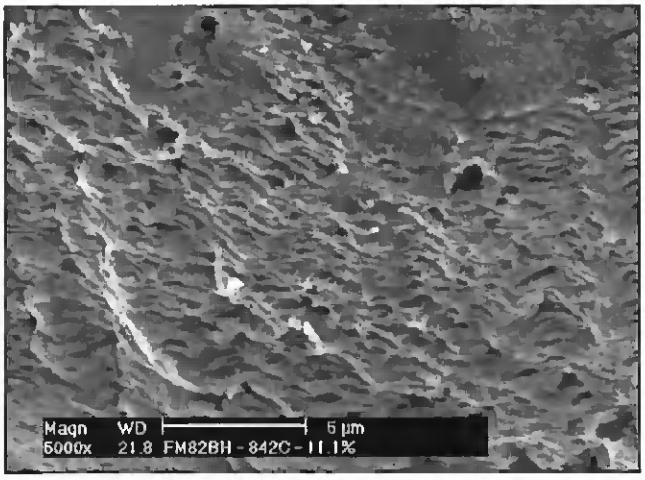

Fig. 3 — Filler Metal 82 fractograph at 842°C and 11% strain (5000×).

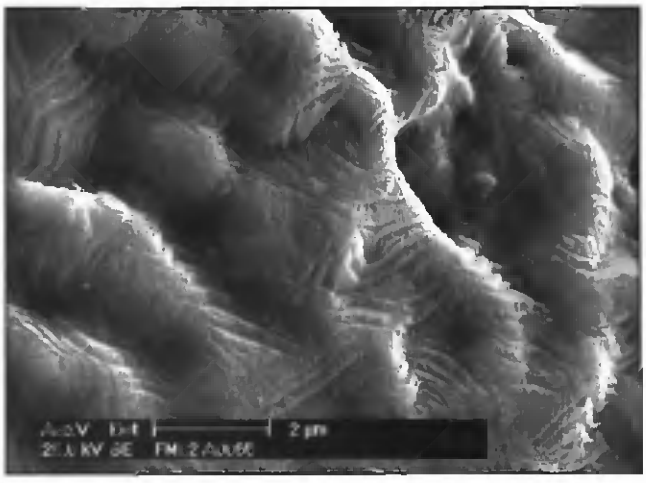

Fig. 4 — Filler Metal 82 fractograph at 1147°C and 11% strain (10,000×; note the serrated, terrace-like patterns across the rounded ductile dimple tG features).

ishing and etching techniques. The use of an electrolytic 10% chromic acid solution revealed the general microstructure and grain boundary constituents. A voltage of 2.5 V, at times ranging from 15 to 20 s, was typical.

Results

Fracture Surface Characterization — SEM

Scanning electron microscopy (SEM) was used to characterize DDC fracture surfaces. As shown in the following figures, the fracture morphologies and features are strikingly similar at analogous temperatures for both Filler Metal 52 and Filler Metal 82.

Low-Temperature Region — The fracture surface in Fig. 1 is representative of intergranular fracture with ductile dimples (termed ductile intergranular). Note that the ductile dimple features are relatively sharp in nature, revealing a considerable amount of microductility. These features are typical of the low temperature region (625–800°C) of the DTR for Filler Metal 52 and Filler Metal 82. As temperature decreases within the low-temperature region of the overall DTR, the flatness of the fracture surface increases from a macroscopic standpoint.

Medium-Temperature Region — The fracture surface in Fig. 2 also exhibits a partially ductile intergranular morphology with a flat appearance macroscopically. Microscopically, the fracture surface is wavy, presenting ductile dimples that become increasingly rounded, suggesting limited microductility as the temperature increases within the medium-temperature region (850–1000°C) of the overall DTR.

Zhang et al. (Refs. 4, 5) described a wavy ductile intergranular fracture feature in Fe-36%Ni weld metals at 900°C that is strikingly similar to the fracture morphology shown in Figs. 2 and 3, with Fig. 3 showing it more clearly at higher magnification. However, although similar in description to the wavy feature described by Zhang, Figs. 2 and 3 could be further characterized as ductile dimples with rounded features. Zhang concluded that the wavy ductile intergranular pattern along the fracture surface was nearly equal in size to cavities formed along the grain boundaries observed metallographically. These cavities would eventually link as applied strain increased resulting in intergranular fracture. Zhang also noted that the size of the wavy feature increased with increasing temperature. Similarly, as observed when comparing Fig. 3 (842°C) to Fig. 2 (936°C), the rounded features also appear to increase in size with increasing temperature, which suggests some ductility recovery. Based on the similarities between the fracture surface descriptions and the temperatures at which these features are observed, this suggests that the rounded ductile intergranular sur-

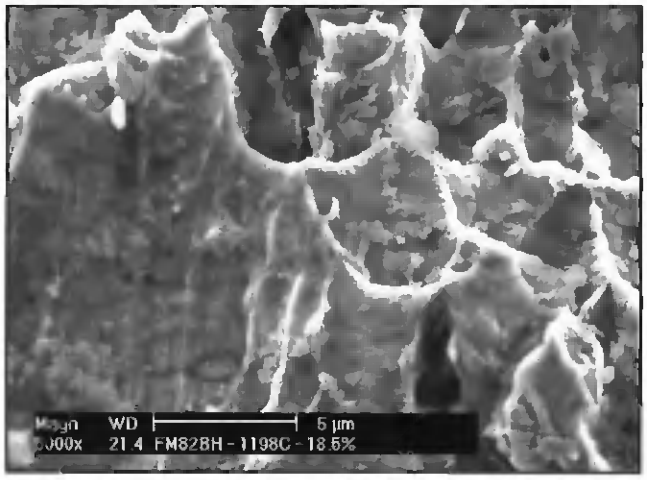

Fig. 5 — Filler Metal 82 fractograph at 1198°C and 18.5% strain (5000×).

face features observed in the medium-temperature region are the result of cavity formation along the migrated grain boundary prior to cavities linking together, eventually resulting in intergranular fracture when subjected to sufficient strain.

High-Temperature Region — The fracture surface in Fig. 4 is representative of the high-temperature region (1050–1200°C) of the overall DTR. This fracture surface appears relatively flat macroscopically (400–600×), with rounded ductile dimple intergranular features evident at higher magnification. Notice that the size of the rounded dimples observed in this high-temperature region is much larger than the size of the ones observed at the medium-temperature region. This indicates the higher level of ductility at higher temperatures, as revealed by the STF test results presented in Part 1. A series of serrated, terrace-like features is evident across the rounded ductile intergranular morphology of the entire fracture surface. These features are evidence of crystallographic planar sliding that has intercepted the fracture surface. Some small particles, possibly MC-carbides, were also observed on the fracture surface, but were too small to identify with energy-dispersive spectrometry (EDS) analysis in the SEM.

As seen in Figs. 4 and 5, as temperature increases within the upper temperature region (1050–1200°C) of the overall DTR, the fracture morphology transitions from rounded ductile dimples to increasingly macroscopically flat with typical sharp ductile dimples microscopically. Additionally, the morphology observed in Fig. 5 is strikingly similar to that observed in the low-temperature region (Fig. 1) of the DTR for both filler materials, as noted by the sharp features of the ductile dimples along the grain faces in both figures. Therefore, fracture surfaces in both the low-temperature (625–800°C) and high-temperature (1050–1200°C) regions of the overall DTR display ductile intergranular morphologies, with evidence of ductile dimples with sharp features at the low and high extremes of the DTR, while also displaying an increase in ductility (Ref. 1). As described in Part I of this investigation, this change in fracture morphology coincides with the restoration of ductility in the low- and high-temperature ranges of the DTR.

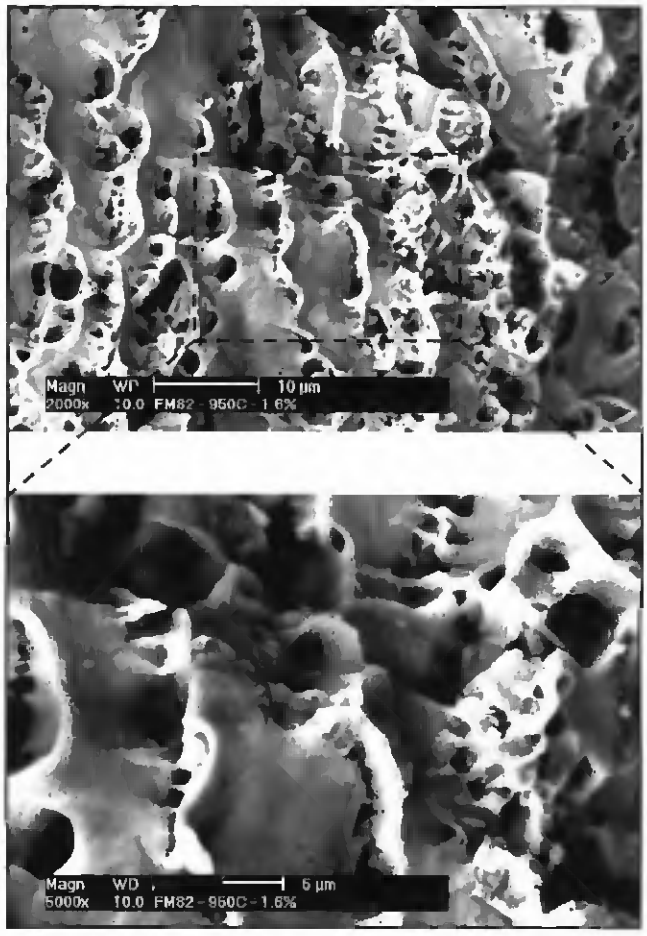

Fig. 6 — Filler Metal 82 fractograph at 950°C and 1.6% strain (hydrogen additions); A — 2000×; B — 5000×.

Filler Metal 82 – Hydrogen Effects — Upon comparing fracture surface morphologies and features for filler materials with and without hydrogen additions and at similar temperatures, some noticeable differences are observed. The fracture surfaces shown in Fig. 6, at 950°C, and Fig. 7, at 1000°C, were taken from STF samples subject to hydrogen additions. These fracture surfaces reveal features different than those observed in the mid-temperature range (850–1000°C) of the overall DTR for weld metal samples with no hydrogen additions. Rather than the characteristic rounded ductile dimple appearance, the presence of hydrogen results in macroscopically (400–600×) flat intergranular fracture, as presented in Fig. 8, with some regions presenting relatively deep voids with porelike features and microvoids. It should be noted that Figs. 6 and 7 were taken from and are representative of discrete regions of the fracture surfaces subject to hydrogen additions, while the remaining regions, as illustrated in Figs. 8 and 9, possess macroscopically (400–600×) flat surface features. At 950°C (Fig. 8), these deep voids actually appear as surface porosity. This feature disappears, however, when the testing is conducted at 1000°C. Overall, the macroscopic flatness of the fracture surface appears to increase with temperature.

The appearance of those deep dimples with porelike features at discrete regions of the overall fracture surface at 950°C coincides with the ductility minimum observed for both heat YN6830 and heat YN7355 of Filler Metal 82 with additions of hydrogen (Ref. 1). A comparison of Figs. 6 and 7 clearly reveals that with only a 50°C increase in temperature, the fracture surface features change dramatically. At 1000°C (Fig. 7), the fracture surface is similar macroscopically to that observed in the high-temperature region (1050–1200°C) of the overall DTR when welded with 100% argon shielding gas, whereas at 950°C (Fig. 6), the morphology is macroscopically flat with porelike features and relatively deep voids at discrete regions of the overall fracture surface. The scattered appearance of these distinctive features

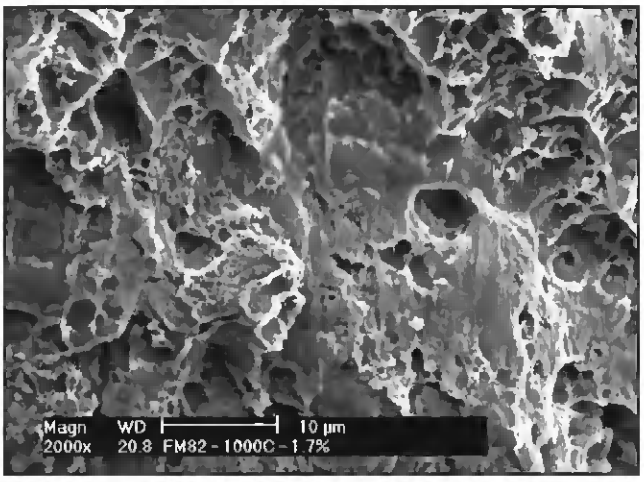

Fig. 7 — Filler Metal 82 fractograph at 1000°C and 1.7% strain (hydrogen additions: 2000×).

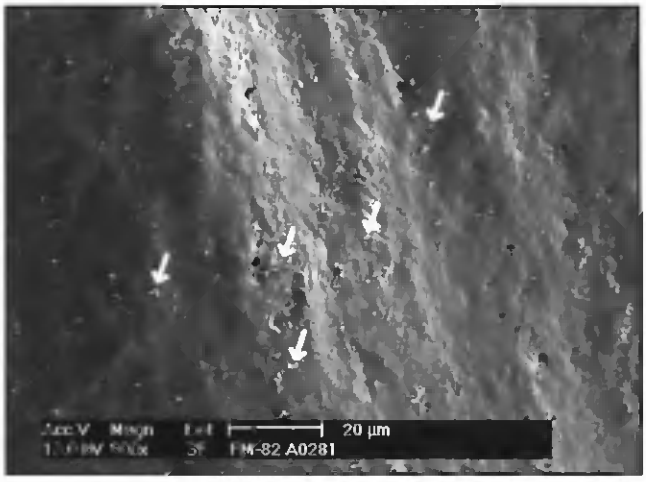

Fig. 8 — Filler Metal 82 fractograph at 950°C and 2% strain (hydrogen additions: 600×). Fracture surface subjected to longer cleaning times, revealing secondary particles.

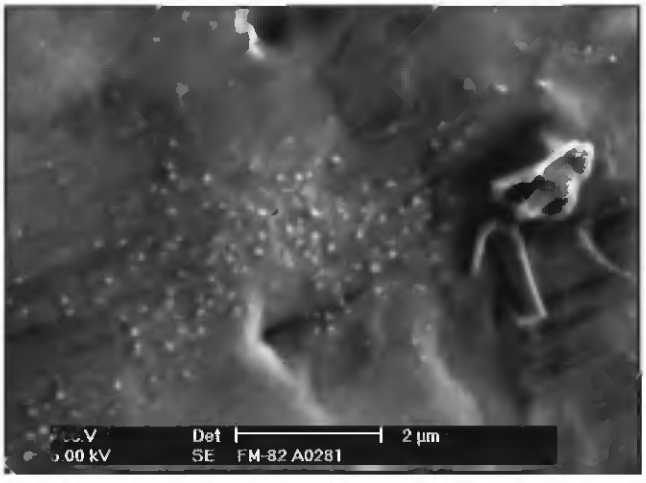

Fig. 9 — Higher magnification Filler Metal 82 fractograph at 950°C and 2% strain (hydrogen additions). Fracture subjected to longer cleaning times, revealing two different sizes of secondary particles.

when larger amounts of hydrogen are present indicates its relationship with the presence of the element in the microstructure. The features possibly indicate that at this temperature, hydrogen diffuses to the grain boundary region, drastically reducing the interface cohesion of the intergranular precipitates with the matrix, resulting in this porelike void formation. Another possibility is that the large amount of hydrogen present at the grain boundaries allows atomic hydrogen to recombine and form molecular hydrogen (H_2), forming microscopic pores along the grain boundary. Furthermore, it is possible that the hydrogen concentration around the grain boundaries reduces the cohesion of the grain boundary itself and triggers hydrogen-enhanced local plasticity (HELP), facilitating void formation at the grain boundaries. It is not clear why the deep voids with porelike features are present at this temperature and not at higher or lower temperatures. Also note the transition from sharp to more rounded ductile dimple features (Fig. 6) similar to that observed on samples not subject to hydrogen additions from the medium-temperature region of the DTR. Furthermore, formation of minor slip intersections across the fracture surface are also observed in Fig. 6 with the intersections increasingly visible at higher magnifications, which may be an indication of the HELP mechanism (see Figs. 6B and 9).

Fracture Surface Precipitates — Despite the fact that all STF tests are run in a protective argon atmosphere, some surface oxidation occurs, which tends to obscure some of the finer details of the fracture surface. The use of a mild inhibited acid solution to remove this oxidation proved very effective in revealing these fine details. When subjected to longer cleaning times, small secondary particles were revealed on the fracture surface. Figures 8 and 9 illustrate the DDC fracture surface of Filler Metal 82 with hydrogen additions at 950°C and 2% strain. Figure 8 is a low-magnification fractograph of the DDC fracture surface revealing large intergranular MC-carbides (between 1–2 µm) throughout (some of these carbides are indicated by arrows), while Fig. 9 provides a higher magnification fractograph of a region of the fracture surface taken from Fig. 8. In Fig. 9, two different distributions of secondary particles are observed. The large particles in Fig. 9 are the same MC-carbides shown in Fig. 8, while the small precipitates, not visible at low magnifications (Fig. 8), appear to be MC-carbides as well. Although Figs. 8 and 9 were taken from the same sample and region, all the cleaned DDC test samples selected from the medium-temperature region (850–1000°C) of the DTR revealed a similar pattern of secondary particles along the fracture surface. Although not always detected by the microscopy methods employed in this study, based on detailed transmission electron microscope (TEM) work performed by subsequent continuing research, precipitation was found to be prevalent along the grain boundaries throughout the entire DTR but at different sizes and quantities (Ref. 6).

Discussion

Fracture Behavior

Table 2 summarizes the fractographic characteristics of Filler Metal 52 and Filler Metal 82 across the entire 625–1200°C DTR. The macroscopic (400–600×) flatness of the fracture surface increases at the low and high temperature extremes of the overall DTR. Ductility recovery at both extremes of the DTR is marked by distinct ductile intergranular fracture that is macroscopically flat with sharp ductile dimple features microscopically. The similarity of this fracture behavior (Figs. 1 and 5) is quite remarkable and apparently results from different mechanisms. As the temperature increases above 625°C into the DDC range, the fracture morphology shifts from macroscopically flat ductile dimple with sharp fea-

tures to rounded ductile dimple features as strain localizes along the migrated grain boundaries. Above 1100°C, the fracture morphology again shifts from the rounded ductile dimple pattern back to macroscopically flat ductile intergranular fracture with sharp ductile dimple features.

In the intermediate temperature region of the DTR, the ductile intergranular fracture surfaces transition first to a ductile dimple pattern with rounded features (Figs. 2 and 3) to a ductile dimple pattern with rounded features revealing distinct crystallographic steps superimposed (Fig. 4). This is clearly evidence of crystalline slip and resultant slip steps that intercept the fracture surface. Zhang et al. (Refs. 4, 5) postulate a wavy pattern that is described to be similar to what has been observed and characterized as rounded ductile dimple features in this study. It is stated that the fracture surface pattern is the result of multiple small voids that form at the intergranular particles, subsequently linking along the migrated grain boundaries and ultimately separating when subject to sufficient strain. Similarly, the rounded ductile dimple features noted on the fracture surface in Filler Metal 52 (Fig. 2) also exhibit numerous small precipitates within a comparable temperature range as that observed by Zhang. These intergranular precipitates participate in the void nucleation process, which explains their presence on the fracture surface with the rounded ductile dimple morphology. Likewise, at a comparable temperature as Fig. 2, Figs. 8 and 9 reveal widespread precipitation on the Filler Metal 82 fracture surfaces. The interaction of these intergranular precipitates and the slip bands observed across the rounded ductile dimples eventually progress to void nucleation and thus participation in the intergranular DDC initiation and/or propagation phenomena through cavity formation and subsequent linking of the cavities through a grain boundary sliding mechanism. However, based on the fracture surface analysis conducted to date, the actual mechanism for void nucleation and propagation and the importance of particle type and size on these mechanisms remain unclear. The effect of carbide type and distribution along migrated grain boundaries in these weld metals is the subject of continuing research (Ref. 6).

Hydrogen Effects on Fracture Behavior

In Part I of this investigation, hydrogen was shown to have a pronounced negative effect on the STF behavior of Filler Metal 82. Hydrogen cracking typically is not a concern in fully austenitic structures based on the high solubility of hydrogen and its low diffusivity in the austenitic (FCC) matrix. Regardless, atomic hydrogen is an extremely mobile interstitial addition and hydrogen cracking may occur in austenitic materials if sufficient hydrogen is present. For example, hydrogen-induced SCC of nickel-based alloys occurs in primary piping of nuclear reactors, where high concentrations of hydrogen (between 20 and 80 ppm by weight of hydrogen for Alloy 600) may be achieved at the crack tip as a result of a cathodic reaction (Ref. 7).

There are two phenomena involved in the hydrogen embrittlement of Ni-based alloys, namely hydrogen-enhanced local plasticity (HELP) (Ref. 8) and hydrogen-induced decohesion (HID) (Ref. 9). The decohesion theory for hydrogen cracking may help explain the increase in DDC susceptibility upon adding hydrogen to the weld pool (Refs. 10, 11). According to this theory, hydrogen diffuses to regions of the crystal lattice where tensile stress concentrations occur. Hydrogen diffusing through a metal lattice accumulates most easily at metallurgical inhomogeneities, or "traps." In the case of DDC, there may exist a critical temperature within the overall DTR where "detrapping" occurs, releasing atomic hydrogen into the grain boundary or intergranular precipitate interfaces, subsequently decreasing grain boundary and interface cohesion that leads to intergranular fracture. Additionally, triple-point grain boundary intersections may be classified as shallow, reversible traps. These particular traps permit rapid hydrogen transport to the crack tip resulting in a critical concentration of hydrogen necessary to initiate cracking, further enhancing fracture under low orders of strain (Ref. 12). Triple-point grain boundary intersections are locations with high stress concentration factors and have been shown through both metallographic and SEM characterization (without hydrogen additions) to be highly susceptible to DDC (Ref. 1).

Alternatively, the hydrogen-enhanced local plasticity (HELP) phenomenon causes cracking based on deformation concentration around the grain boundaries where the plasticity has been enhanced by the high hydrogen content in those regions. As a result, lower macroscopic strains are necessary to initiate mi-

Table 1 — Chemical Composition of Filler Materials (wt-%)

Element	Filler Metal 52 Heat NX9277	Filler Metal 82 Heat YN6830	Filler Metal 82 Heat YN7355	Filler Metal 82 Heat YB7724
C	0.026	0.04	0.04	0.041
Mn	0.25	2.86	2.75	2.79
Fe	8.88	1.18	0.70	0.90
S	0.0037	0.01	0.002	0.001
Si	0.17	0.12	0.07	0.06
Cu	0.011	0.09	0.07	0.04
Ni	60.12	72.75	72.8	72.98
Al	0.71	N/A	N/A	0.05
Ti	0.50	0.37	0.47	0.45
Cr	29.09	20.1	20.1	19.98
Cb + Ta	0.02	2.3	2.6	2.7
Mo	0.05	N/A	N/A	N/A
P	0.0044	0.007	0.01	0.004
Pb	0.0001	0.004	0.002	0.002
Co	—	0.05	0.04	0.01

Table 2 — Summary of Fractographic Characteristics

Temperature Range	Fracture Characteristics
Low 625–800°C	Macroscopically flat ductile intergranular with ductile dimples with sharp features.
Medium 850–1000°C	Ductile intergranular with rounded ductile dimple surface features (small dimples and voids).
High 1050–1200°C	Macroscopically flat with crystallographic planar sliding evident across rounded ductile dimple fracture surface features. Transitions to macroscopically flat intergranular with ductile dimples with sharp features as temperature increases at the high end of the ductility trough.

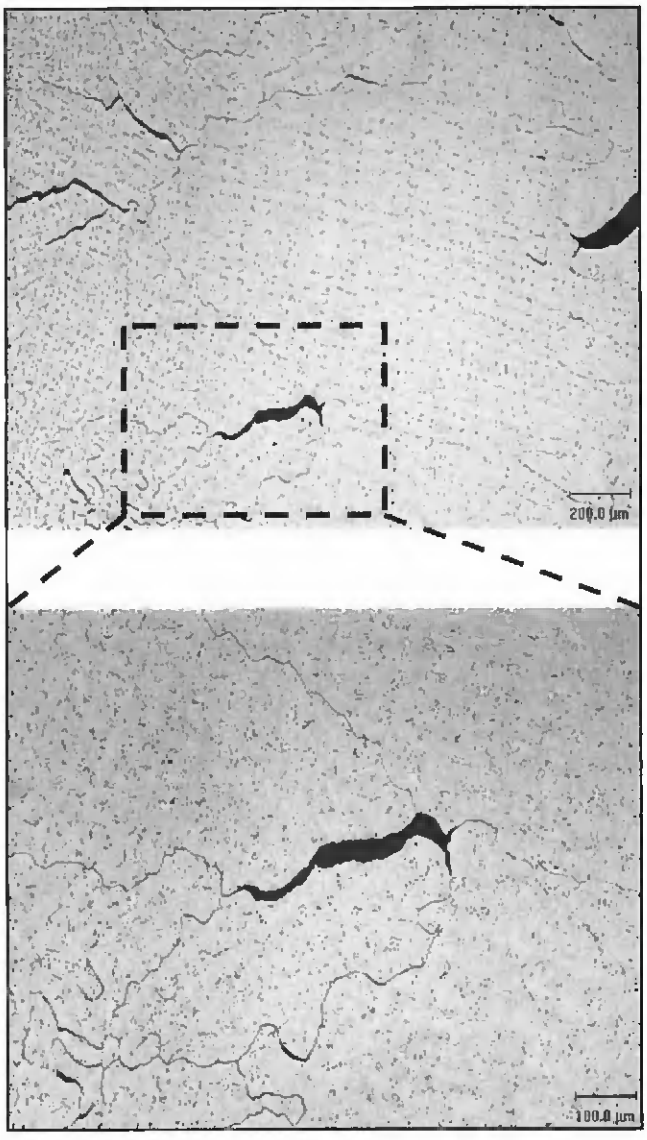

Fig. 10 — Ductility dip cracking along triple-point grain boundary intersections (hydrogen additions).

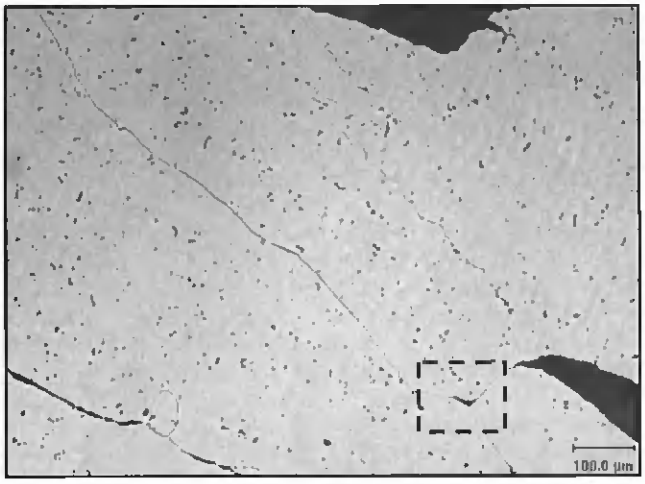

Fig. 11 — Ductility dip cracking along triple-point grain boundary intersections (hydrogen additions). (Note: the boxed area shows crack initiation at the grain boundary intersection.)

crocracks. The hydrogen enrichment around the grain boundaries promotes heterogeneous planar slip, which causes further strain concentration around the grain boundaries, resulting in void formation (Ref. 13), as shown in Fig. 9. Notice that the fracture surface in Fig. 9 has been submitted to acidic cleaning for long periods of time to reveal the intergranular precipitates present on the fracture surface. As a result of this extensive chemical cleaning, the fracture surface has become somewhat etched, resulting in the terraces caused by the slip bands becoming blurry. Interestingly, the fracture morphology illustrated in Fig. 4 on a sample not subject to hydrogen additions reveals distinct similarities to those described by the HELP mechanism above. As temperature increases within the DTR, the rounded ductile dimple features transition to rounded ductile dimple with serrated, terrace-like features across the dimples similar to those observed on the fracture surface in Figs. 4 and 9. Perhaps similar grain boundary sliding mechanisms are occurring, suggesting that the HELP mechanism enhances DDC at lower applied strain levels.

Optical microscopy was performed to determine if, in fact, the frequency of DDC at triple-point grain boundary intersections increased when the weld metal microstructure was subject to additions of hydrogen. Figures 10 and 11 reveal cracking along triple-point grain boundary intersections in Filler Metal 82 microstructures subject to hydrogen additions. Based on metallographic observations, the frequency of DDC near triple-point grain boundary intersections increases when adding hydrogen to the weld metal microstructure. All of the cracks observed in Fig. 10 reveal cracking at triple-point grain boundary intersections. The higher magnification micrograph in the bottom portion of Fig. 10 clearly shows cracking between three triple-point grain boundary intersections, with the crack width at a maximum near the intersections. At relatively low levels of strain (less than 3%), cracking occurs almost exclusively at these intersections, supporting the hypothesis that hydrogen diffuses to regions of the crystal lattice where tensile stress concentrations occur, decreasing grain boundary cohesion and ultimately increasing DDC susceptibility. Diffusion of hydrogen to highly stressed triple-point grain boundary intersections is further supported by Fig. 11. The boxed area in this figure reveals a minor opening at the boundary intersection, supporting decreased grain boundary cohesion based on high hydrogen contents at highly stressed grain boundary intersections.

Interestingly, the temperature range at which these metallographs were taken (950°C) is similar to the temperature (900°C) at which Zhang et al. (Refs. 4, 5) observed cracking caused by precipitation-induced cavity nucleation and subsequent cavity propagation and linking from a grain boundary sliding mechanism at triple-point grain boundary intersections. Perhaps the grain boundary sliding and void formation phenomena are enhanced by the presence of hydrogen, which easily diffuses to locations of high stress concentration, resulting in initiation of the grain boundary sliding mechanism and assisting void nucleation at lower applied strain levels.

The fracture surface shown in Fig. 6, which corresponds to Filler Metal 82 strained 1.6% at 950°C, is macroscopically flat with relatively deep voids and porelike features within discrete regions of the overall fracture surface, whereas at 1000°C (Fig. 7), these particular features disappear, transitioning toward a macroscopically flat intergranular ductile fracture surface with typical ductile dimples. These relatively deep voids with porelike features within discrete regions possibly indicate that at this temperature, hydrogen diffusion to the grain boundary is maximized allowing hydrogen interaction with the precipitates triggering the HID and HELP mechanisms. The interactions of HID and HELP at the intergranular precipitates and matrix interfaces along with grain boundary sliding result in the for-

mation and growth of voids with very low applied strains. The large and deep voids are thought to have formed around the large and medium precipitates, while the microdimples have formed around the small precipitates. As previously mentioned, it may be possible that the deep dimples with porelike features have formed due to the recombination of atomic hydrogen at the grain boundaries to form molecular hydrogen (H_2).

Diffusion is an exponential function of temperature ($D = D_0 e^{-RT}$). Based on its high diffusivity, hydrogen moves easily through the microstructure. Perhaps as temperature increases beyond the critical temperature for maximum hydrogen "detrapping," hydrogen diffuses out of the microstructure, resulting in a reduction of porelike features at hydrogen trap locations such as grain boundaries. Thus, the possible reason for the observed decline in porelike features at 1000°C vs. 950°C is simple diffusion of interstitial hydrogen away from the grain boundary. Unlike STF samples welded with 95Ar-5H_2 shielding gas, Filler Metal 52 and Filler Metal 82 samples welded with 100% argon shielding reveal no evidence of porelike features across the fracture surfaces, and the strain necessary to induce cracking was found to be significantly higher. The effect of hydrogen on boundary properties and fracture behavior is the subject of continuing research (Ref. 6).

Conclusions

Filler Metal 52 and Filler Metal 82 have similar fractographic characteristics throughout the DTR.

Ductility dip cracking fracture morphology can be separately classified into low (625–800°C), medium (850–1000°C), and high (1050–1200°C) temperature ranges within the DTR. At the low and high temperature extremes, the fracture morphology is described as ductile intergranular with ductile dimples with sharp features. In the medium-temperature range, the ductile dimple intergranular fracture surface features have a rounded appearance.

The fracture surface exhibits distinct crystallographic slip intersections at the low end of the high-temperature range (1050–1150°C) of the DTR.

Hydrogen additions significantly increased susceptibility to DDC. This increased susceptibility was characterized by crack initiation at grain boundary triple points generating an intergranular macroscopically flat fracture surface and some evidence of deep voids with porelike features within a narrow temperature range.

Acknowledgments

The authors would like to thank Nathan Nissley, Dan Ryan, and Shu Shi, members of the Welding and Joining Metallurgy Group at The Ohio State University, for their valuable assistance during this investigation. We are grateful for the financial support of this investigation by BWX Technologies, Inc., and to Jeff Kikel of BWXT for helpful discussions and insight.

References

1. Collins, M. G., and Lippold, J. C. 2003. An investigation of ductility dip cracking in nickel-based filler materials — Part 1. *Welding Journal* 82(10): 288-s to 295-s.

2. Hemsworth, B., Boniszewski, T., and Eaton, N. F. 1969. Classification and definition of high-temperature welding cracks in alloys. *Metal Construction and British Welding Journal.* pp. 5–16.

3. Honeycombe, J., and Gooch, T. G. 1970. Microcracking in fully austenitic stainless steel weld metal. *Metal Construction and British Welding Journal* (9): 375–380.

4. Zhang, Y., Nakagawa, H., and Matsuda, F. 1985. Weldability of Fe-36%Ni alloy (Report V) — Behaviors of grain boundary sliding and cavity formation preceding reheat hot cracking in weld metal. *Transactions of JWRI*, 14/2(12):2 (12): 119–124.

5. Zhang, Y., Nakagawa, H., and Matsuda, F. 1985. Weldability of Fe-36%Ni Alloy (Report VI) — Further investigation on mechanism of reheat hot cracking in weld metal. *Transactions of JWRI* 14/2 (12).

6. Ramirez, A. J. 2002. Unpublished research performed at Ohio State University.

7. Estman, J., Matsumoto, T., Narita, N., Heubaum, F., and Birnbaun, H. K. 1980. Hydrogen effects in nickel — embrittlement or enhanced ductility. *Hydrogen Effects in Metals.* Warrendale, Pa.: TMS, pp. 397–409.

8. Symons, D. M. 1999. The effect of hydrogen in the fracture toughness of Alloy X-750 at elevated temperatures. *Journal of Nuclear Materials* 265: 225–231.

9. Troiano, A. R. 1960. The role of hydrogen and other interstitials in the mechanical behavior of metals. *Trans. ASM* 52(1): 54–80.

10. Savage, W. F., Nippes, E. F., and Szekeres, E. S. 1976. Hydrogen-induced cracking in a low alloy steel. *Welding Journal* 55: 276-s to 283-s.

11. Jones, D. A. 1996. *Principles and Prevention of Corrosion*, 2d ed. Upper Saddle River, N.J.: Prentice & Hall, Inc.

12. Mills, W. J., and Brown, C. M. 2001. Fracture toughness of Alloy 600 and EN82H weld in air and water. *Metallurgical Transactions A* 32A(5): 1161–1174.

13. Matsuda, F. 1990. Hot crack susceptibility of weld metal. *Proceedings of the 1st U.S.–Japan Symposium on Advances in Welding Metallurgy.* Miami, Fla.: American Welding Society, pp. 19–36.